Esketamine attenuates bone cancer pain by suppressing MAPK signaling and glial activation in the spinal dorsal horn of rats

Liang Cheng, Dongjie Wang, Zhiqiang Zhang, Yu Zhang, Yunyun Tang, Kuibin Bao, Bin Guo, Kaijing Zhang, Yu Chen, Hui Ren, Chengfei Xu & Huadong Ni

We are providing an unedited version of this manuscript to give early access to its findings. Before final publication, the manuscript will undergo further editing. Please note there may be errors present which affect the content, and all legal disclaimers apply.

If this paper is publishing under a Transparent Peer Review model then Peer Review reports will publish with the final article.

Esketamine Attenuates Bone Cancer Pain by Suppressing MAPK Signaling and Glial Activation in The Spinal Dorsal Horn of Rats

Liang Cheng[1], Dongjie Wang[2], Zhiqiang Zhang[1], Yu Zhang[1], Yunyun Tang[1], Kuibin Bao[1], Bin Guo[1], Kaijing Zhang[1], Yu Chen[1], Hui Ren[1], Chengfei Xu[2,3]*, Huadong Ni[2]*

1. Department of Anesthesiology, The Third People's Hospital of Bengbu, 38 Shengli Middle Road, Bengbu, China, 233000

2. Department of Anesthesiology and Pain Research center, The Affiliated Hospital of Jiaxing University, 1882 Zhonghuan South Road, Jiaxing, China, 314001

3. Department of Anesthesiology, Bengbu Third People's Hospital Affiliated to Bengbu Medical University, Bengbu, China, 233000

Correspondence:

Chengfei Xu, Email: bbxcfpain@163.com

Huadong Ni, Email: huadongni@zjxu.edu.cn

Abstract

Bone cancer pain (BCP) is a debilitating condition driven by spinal

neuroinflammation and glial activation. Esketamine (ESK), an NMDA receptor antagonist, exhibits analgesic effects beyond receptor blockade, but its mechanisms in BCP remain unclear. Here, a rat BCP model was established by intramedullary injection of Walker 256 cells, followed by intrathecal ESK administration (20, 40, 60 μg). Pain behavior was assessed using Von Frey, Hargreaves, CatWalk, and open field tests. While histology confirmed tumor-induced osteolysis, ESK did not prevent bone destruction. Instead, ESK significantly reduced mechanical and thermal hypersensitivity, improved gait and anxiety-like behaviors, and suppressed microglial and astrocytic activation in the spinal dorsal horn. This was accompanied by reduced pro-inflammatory cytokine levels and inhibition of MAPK pathway activation. Pharmacological blockade of glia (fluorocitrate, minocycline) or MAPK signaling (SB203580, SP600125) reproduced these effects, confirming the contribution of glia-MAPK interactions. These findings indicate that ESK alleviates BCP by suppressing glial-driven neuroinflammation and MAPK signaling, highlighting its potential as a multimodal analgesic.

Keywords: bone cancer pain, spinal dorsal horn, esketamine, glial activation, MAPK

1. Introduction

Bone cancer pain (BCP) constitutes a debilitating condition affecting patients having primary and metastatic bone tumors, significantly impairing their quality of life[1]. It is characterized by a complex interplay of nociceptive, inflammatory, and neuropathic pain mechanisms, making its management particularly challenging[2-4]. Current analgesic strategies, including opioids and nonsteroidal anti-inflammatory drugs (NSAIDs), often provide insufficient relief and are associated with severe adverse effects such as tolerance and addiction[5, 6]. Therefore, there is an urgent need for novel treatment approaches to efficiently alleviate BCP while minimizing side effects.

Esketamine (ESK), the S(+)-enantiomer of ketamine, represents an N-methyl-D-aspartate (NMDA) receptor antagonist with well-documented analgesic and anti-inflammatory properties[7-9]. Beyond its action on NMDA receptors, recent studies have suggested that ESK modulates glial cell activity and neuroinflammatory pathways[10-13], which is crucial in chronic pain pathogenesis. Particularly, both microglia and astrocyte activation in the SDH contribute to central sensitization and pain signal amplification in BCP[14, 15]. Microglia produce pro-inflammatory cytokines: IL-1β, IL-6 and TNF-α, further exacerbating pain hypersensitivity[16]. Concurrently, activated

astrocytes release additional inflammatory mediators, promoting neuronal hyperexcitability and persistent pain states[17].

One of the key intracellular pathways involved in glial activation and neuroinflammation is the mitogen-activated protein kinase (MAPK) pathway, which includes c-JNK, p38, and ERK[18]. The MAPK pathway activation produces inflammatory cytokines and amplifies nociceptive signaling[19, 20]. Given its multifaceted pharmacological profile, ESK may exert its analgesic effects in BCP by suppressing glial activation, reducing inflammatory cytokine expression, and inhibiting MAPK pathway activation. However, the precise dose-dependent effects of ESK on these mechanisms in BCP remain vague.

Our aim was to assess the analgesic effects of ESK on BCP as well as its underlying mechanisms. Additionally, we established a BCP rat model and administered continuous intrathecal injection of ESK at different doses. By elucidating the dose-dependent effects of ESK on glial cell activity, neuroinflammation, and MAPK pathway modulation, we provide innovative perspectives into the potential mechanisms behind ESK as an effective analgesic for BCP. These findings may pave the way for future therapeutic strategies targeting glial inhibition and neuroimmune modulation in managing chronic cancer pain.

2. Materials and Methods

2.1 Animals

Female Sprague-Dawley rats (180-200 g, the Experimental Animal Center of Zhejiang Province Academy of Medical Sciences, Hangzhou, China) were habituated at 22 ± 2°C, 12-h light/dark cycle, with unrestricted food and water access. Each cage housed six to eight rats, and all experiments were conducted during the daytime, making all efforts to minimize the used animal number and reduce potential distress. All behavioral tests were conducted between 9:00 a.m. and 6:00 p.m., and to eliminate observer bias, experimenters responsible for the evaluations were blinded to the experimental conditions and treatment assignments. All methods are reported in accordance with ARRIVE guidelines. Furthermore, the research adhered to the guidelines established by the International Association for the Study of Pain. In accordance with the Guidelines for the Care and Use of Laboratory Animals and the ethical approval (Approval No.: JXYY2024-056) from the Animal Ethics Committee of Jiaxing University, all rats were humanely euthanized at the experimental endpoint (day 18 after tumor inoculation) or when they met predefined humane endpoints (e.g., tumor-induced severe distress, significant weight loss > 20%, or impaired mobility). At the end of the experiment, rats were euthanized

by an overdose of isoflurane inhalation in accordance with the *Euthanasia Guidelines M79/1222 (CULATR, Dec 2022)*. This method was selected for its rapidity, reliability, and minimal suffering to animals.

2.2 Preparation of cells

Walker 256 breast cancer cells were obtained from the Cell Culture Center of the Chinese Academy of Medical Sciences (Beijing, China) and maintained in Dulbecco's Modified Eagle Medium (DMEM) supplemented with 10% fetal bovine serum (FBS) at 37 °C in a humidified incubator containing 5% CO_2. For ascites induction, 0.5 ml of cell suspension (5×10^6 cells/ml) was injected into the peritoneal cavity of rats weighing 60-80 g. After ascitic fluid collection, cells were isolated by centrifugation and washed three times with pre-cooled phosphate-buffered saline (PBS). The final cell pellet was resuspended in PBS to a concentration of 1×10^5 cells/μl for subsequent use.

2.3 BCP model

As in our previous studies[21], rats were anesthetized with 2%-3% isoflurane. A sterile incision was made in the lower third of the left tibia, and a 0.8-mm hole was drilled into the tibial medullary cavity using a high-speed drill. The BCP group was intramedullary injected with 10 μl Walker 256 cells (1×10^6), while the sham group was

injected with heat-killed Walker 256 cells. A fixed Hamilton microsyringe was used to ensure precise and controlled delivery of cells, with the syringe held in place for 2 min to prevent cell leakage. Immediately after injection, bone wax was used for hole sealing, and the surgical site was sutured. Postoperative monitoring was conducted to ensure proper recovery, and animals were observed for signs of distress or infection.

2.4 *Von* Frey test

Mechanical allodynia was determined using the *Von* Frey test to measure paw withdrawal responses to mechanical stimuli. Before testing, rats were handled daily for three consecutive days to acclimate them to the experimental environment[22]. On the test day, rats were placed in transparent wire-meshed floor Plexiglas compartments (25 × 20 × 20 cm) and acclimated for half an hour. Mechanical stimuli were applied to the hind paw using *Von* Frey monofilament (BME-404; Biological Medicine Institute, Beijing, China) following the up-down method, thereby recording the paw withdrawal threshold (PWT), repeating the measurements five times at 10-s intervals, and calculating the average PWT. To ensure unbiased evaluation, blinded researchers conducted the behavioral assessments.

2.5 Thermal hyperalgesia

The thermal hyperalgesia was determined with the Hargreaves test to measure paw withdrawal latency (PWL) responding to a radiant heat stimulus[23]. Rats were positioned in transparent Plexiglas compartments on a heated glass surface and acclimated for half an hour before testing. A focused infrared beam (IITC Life Science, USA) was directed at the ipsilateral hind paw plantar surface, recording the time taken for the rat to withdraw its paw as PWL, repeating measurements five times at 10-s intervals, and calculating the average PWL. To ensure animal safety and prevent tissue damage, we established a cutoff time of 20 s. To ensure unbiased evaluation, blinded researchers conducted the behavioral assessments.

2.6 Rotarod Testing

To evaluate potential motor impairments induced by intrathecal injection of ESK, rotarod testing was carried out using an accelerating rotarod apparatus (Ugo Basile, Varese, Italy)[24]. Before baseline testing, animals were subjected to a habituation protocol consisting of daily 3-min training sessions for at least 5 days. During testing, rats were positioned on a rotarod (70 mm diameter) linearly accelerated from 4 to 40 rpm over a maximum cutoff time of 3 min, recording the latency to fall from the rod. Data were normalized and reported as a

percentage of the baseline performance for each experimental group. This approach ensured accurate assessment of motor coordination while controlling for inter-individual variability.

2.7 CatWalk analysis

Gait analysis was performed using the CatWalk automated system to assess pain-related locomotor behaviors in freely moving rats[25]. This system tracks voluntary movement along an enclosed runway, with a high-speed camera under a glass floor capturing real-time paw prints. To ensure data reliability, a minimum of four consecutive step cycles or complete tunnel passages were recorded per rat. Pain-related gait alterations were assessed using four key parameters: max contact area, mean intensity, single stance, and swing. To minimize variability, gait asymmetry was quantified using the left/right hind paw (LH/RH) ratio, allowing for a more precise evaluation of pain-induced changes in locomotor function.

2.8 Open Field Test (OFT)

Here, OFT was conducted to determine exploratory behavior and anxiety-like responses[26]. To evaluate locomotor coordination and anxiety-like behavior, rats were individually placed in an open field arena (100 × 100 × 50 cm) situated in a softly lit environment with ambient temperature approximating their natural habitat. Each

session lasted 10 minutes under low-light conditions, during which exploratory activity was recorded via an overhead high-speed camera. Behavioral parameters, particularly time and distance traveled in the central zone, were analyzed using Jiliang Behavior Analysis Software (Shanghai, China). All animals underwent a two-day habituation period prior to behavioral assessment. To minimize bias, all experiments were performed in a blinded manner. After each trial, the open field apparatus was thoroughly cleaned with alcohol wipes to eliminate residual odor and feces, thereby preventing olfactory interference with subsequent subjects.

2.9 Micro-CT Analysis

To verify tumor establishment in the tibia, CT scans were performed on day 12 following tumor cell inoculation. A SOMATOM CT scanner (Siemens, Germany) was employed to conduct high-resolution 3D reconstructions of the rat tibia. In reference to previous protocols[27], scanning parameters were configured as follows: tube voltage 120 kVp, helical acquisition mode, 1 mm slice thickness and interval, Care Dose 4D technique, and U30u kernel with a medium-smooth reconstruction algorithm. The field of view was set to 100 mm, suitable for detailed skeletal imaging in SD rats. Image processing and reconstruction were completed using the Siemens Syngo

MultiModality Workplace (MMWP) workstation.

2.10 Histological analysis

Following euthanasia, the ipsilateral tibia was carefully excised and fixed in 4% PFA at 4 °C for preservation. The specimens were then demineralized in 10% EDTA for 24 h, dehydrated, and paraffin-embedded. Coronal sections (8 μm) were obtained utilizing a microtome and stained with H&E to assess bone structure, tumor infiltration, and osteolysis. Images were taken under an Olympus BX51 microscope with 20× and 40× objectives for detailed histopathological evaluation.

2.11 Drugs and administration

ESK was purchased from Jiangsu Hengrui Pharmaceutical Co., Ltd. (Jiangsu, China) and administered intrathecal injection (i.t.) at concentrations of 20, 40, or 60 μg. The doses of esketamine were selected based on previous studies[10]. It was diluted with sterile normal saline. To investigate the role of glial cells, fluorocitrate (10 nmol/10 μl; Sigma-Aldrich, USA) and minocycline (100 nmol/10 μl; Yuanye Biotech, China) were used as selective astrocyte and microglial inhibitors, respectively. As in our previous study[28], fluorocitrate was initially solubilized in 1 M hydrochloric acid and subsequently diluted with saline. Minocycline was freshly dissolved in saline immediately before

administration, with mild heating in a water bath to ensure complete dissolution. Both compounds were freshly prepared in conditions prior to use. To assess MAPK pathway involvement, the JNK inhibitor SP600125 (5 µg/10 µl; Cell Signaling Technology, USA) and the p38 inhibitor SB203580 (10 µg/10 µl; Abcam, UK) were dissolved in DMSO to a final DMSO concentration of 1%. Intrathecal drug delivery was performed via a pre-implanted PE-10 (0.28 mm inner diameter and 0.61 mm outer diameter) catheter inserted into the L4-L5 subarachnoid space, as previously described. Rats were briefly anesthetized with isoflurane prior to injection. All drugs were administered once daily from POD 13 to 16 in a volume of 10 µl, followed by a 5-µl Saline flush. Control animals received equivalent volumes of saline or vehicle. After drug administration, rats were housed individually and monitored for signs of distress, motor dysfunction, or adverse effects. Standard food and water were provided throughout the study period.

2.12 Western Blotting (WB)

Rats were anesthetized with 2–3% isoflurane, and the ipsilateral spinal cord segments (L3–L5) were rapidly dissected and collected on ice. The tissues were homogenized in RIPA lysis buffer (containing protease and phosphatase inhibitors) using an ultrasonic homogenizer.

The homogenates were centrifuged at 14,000 rpm for 20 min at 4 °C, and the supernatants were collected. Protein concentrations were determined using a BCA protein assay kit (Biyuntian Biotechnology Institute, China). Equal amounts of protein (40 µg per lane) were separated on 10% SDS–PAGE gels and transferred onto PVDF membranes. The membranes were blocked with 5% nonfat milk for 2 h at room temperature and then incubated overnight at 4 °C with the following primary antibodies (all diluted 1:1000): Iba-1 (ab283319, Abcam), ERK (ab184699, Abcam), phospho-ERK (ab278538, Abcam), GFAP (C9205, Sigma), JNK (sc-571, Santa Cruz), phospho-JNK (sc-81502, Santa Cruz), p38 (AF6456, Affinity), phospho-p38 (AF4001, Affinity), IL-1β (AF5103, Affinity), IL-6 (DF6087, Affinity), TNF-α (AF7014, Affinity), and β-actin (AF7018, Affinity). After three washes with TBST, the membranes were incubated with HRP-conjugated secondary antibodies (BL001A or BL003A, Biosharp; 1:3000 dilution) for 2 h at room temperature. Protein bands were visualized using an enhanced chemiluminescence reagent and imaged with a Bio-Rad gel documentation system. Band intensities were quantified using ImageJ software and normalized to β-actin to calculate relative protein expression levels.

2.13 ELISA

ELISA kits for quantifying IL-1β (PI303), IL-6 (PI328), and TNFα (PT516) were obtained from Beyotime (Shanghai, China). The IL-1β, IL-6, and TNFα levels in rat spinal cord tissues were quantified using commercial ELISA kits (Beyotime, China). Spinal cord tissues were subjected to homogenization in RIPA buffer that contained protease and phosphatase inhibitors, determining total protein concentration with a BCA Protein Assay Kit (Beyotime, China). After quantification, 100 μg of total protein was used for ELISA per the protocols. Optical density was assessed at 450 nm via a microplate reader, normalizing cytokine concentrations to total protein content.

2.14 Immunofluorescence (IF) Staining

Twelve days after BCP surgery, rats were subjected to deep anesthesia and transcardial perfusion with 0.9% saline, followed by 4% PFA[29]. The lumbar SDH segments were instantly dissected and post-fixed in 4% PFA for 6 h prior to dehydration in 15%–30% sucrose solutions at 4 °C for 48 h. Tissues were embedded in the OCT compound and sliced at 16 μm with a cryostat. Sections were incubated overnight at 4 °C with primary antibodies, including Iba-1 (1:300, Abcam), GFAP (1:400, Sigma), IL-6 (1:100, Affinity), IL-1β (1:100, Affinity), and TNFα (1:100, Affinity). The sections were rinsed and incubated with fluorescently conjugated secondary antibodies (1:500, Abcam): Alexa Fluor 488

donkey anti-rabbit (ab150073, Abcam), 488 donkey anti-goat (ab150129, Abcam) and 594 donkey anti-mouse (ab150108, Abcam) for 50 min at room temperature. Counterstaining nuclei with DAPI (Invitrogen) was followed by capturing images with a confocal laser scanning microscope.

2.15 Statistical Analysis

Statistical analyses were performed using GraphPad Prism (v9.5). Sample sizes were based on previous studies; data are presented as mean ± SEM. Differences between two groups were assessed by two-tailed unpaired Student's test. Comparisons across multiple groups or time points used one-way or two-way ANOVA, respectively, with Tukey's post hoc test where applicable. Statistical significance was set at $P < 0.05$.

3. Results

3.1. BCP model establishment and dose-dependent analgesic effects of ESK

As shown in **Figure 1A**, a rat model of BCP was established in accordance with previously reported protocols[30]. Both 3D-CT imaging and H&E staining results confirmed tumor-induced bone destruction in the BCP group while showing no structural abnormalities in the Sham group (**Figure 1B and C**). Behavioral assessments **(Figure 1D**

and E) demonstrated that by POD12, the BCP group exhibited significantly decreased PWT and PWL compared to the Sham group, indicating successful model induction. Longitudinal tumor size and body weight of rats after tumor inoculation are shown in Table 1.

To investigate the analgesic effects of ESK, the BCP group received continuous intrathecal injection of ESK (20, 40, 60 μg) from POD 13 to 16. Behavioral test revealed a dose-dependent increase in PWT and PWL in ESK-treated rats **(Figure 1F and G)**, whereas no such improvement was observed in the vehicle-treated BCP group. The highest dose (60 μg) exhibited the most significant effect. To evaluate potential motor impairments following repeated ESK administration, a rotarod test was performed. As shown in **Figure 1H**, no significant motor performance differences were observed between the vehicle and ESK groups under the conditions tested.

To assess the temporal profile of glial activation in BCP, we performed double immunofluorescence staining for Iba-1 and GFAP in the SDH. Iba-1 expression increased from POD6 and remained elevated through POD18, while GFAP expression was significantly upregulated at POD12 and POD18 but unchanged at POD6. Quantitative analysis confirmed early microglial and delayed astrocytic activation **(Figure 1I–K)**. These results are consistent with

previous reports describing sequential glial activation following tumor-induced bone injury[31].

3.2. ESK improves gait performance and anxiety-like behavior

Gait analysis using the CatWalk system revealed significant locomotor impairments in BCP rats in contrast to the Sham group (**Figure 2A**) [32]. Particularly, BCP rats displayed significant gait disturbances, including a reduced maximum contact area, decreased print intensity, prolonged single stance phase, and altered swing duration (**Figure 2B-E**), indicating impaired weight-bearing and movement asymmetry due to pain. In the high-dose ESK group (BCP + ESK-60), these gait parameters were partially improved compared to vehicle-treated BCP rats.

In the OFT test (**Figure 2F**), BCP rats showed decreased exploratory activity and increased anxiety-like behavior, indicating a reduction in both distance and time (**Figure 2G-H**) spent in the center area.These changes suggest heightened pain-related anxiety and avoidance behavior. The ESK administration significantly reversed these effects, increasing both the distance and time in the center area, indicating reduced anxiety-like behavior and improved exploratory activity.

3.3. ESK dose-dependently inhibits microglia and astrocyte

activation

Immunofluorescence analysis revealed marked upregulation of Iba-1 and GFAP in the SDH of BCP rats, indicating pronounced microglial and astrocytic activation (**Figure 3A–C**). Esketamine treatment reduced the expression of both markers in a dose-dependent manner, with the 60 µg group showing the strongest reduction. Morphological assessment further showed hypertrophic changes in Iba-1-positive microglia and GFAP-positive astrocytes in the BCP group, and these changes appeared less pronounced after ESK administration.

The WB analysis corroborated the IF findings (**Figure 3D**). Both Iba-1 and GFAP were significantly increased in the BCP + Vehicle group compared to the Sham group. The ESK dose-dependently diminished both levels, with the highest dose showing the most significant suppression (**Figure 3E and F**). Quantitative densitometric analysis showcased that Iba-1 levels in the BCP group were approximately 2.75-fold higher than in the Sham group, while GFAP levels were 2.30-fold higher. Following ESK administration, Iba-1 expression decreased by 29.2% (low-dose), 46.2% (medium-dose), and 58.3% (high-dose), whereas GFAP expression declined by 17.4% (low-dose), 32.6% (medium-dose), and 47.2% (high-dose).

To further confirm the role of glial cells in inflammatory responses,

BCP rats received continuous intrathecal injection of fluorocitrate (an astrocyte inhibitor) or minocycline (a microglial inhibitor) from POD 13 to 16. As shown in **Figure 3G**, both treatments increased PWT, suggesting alleviation of mechanical allodynia. Immunofluorescence staining revealed that GFAP and Iba-1 expression in the SDH were significantly reduced after respective inhibitor treatments (**Figure 3H to K**). In parallel, Western blot analysis showed that the expression levels of IL-1β, IL-6, and TNF-α were also reduced following glial inhibition (**Figure 3L to O**). These data support an association between glial activation and elevated proinflammatory cytokines during BCP.

3.4. ESK dose-dependently downregulates pro-inflammatory cytokines

The outcomes of ELISA (**Figure 4A to C**) manifested that the BCP group exhibited significantly increased IL-1β, IL-6 and TNF-α levels in contrast to the Sham group, indicating a heightened inflammatory response associated with BCP. The ESK administration dose-dependently suppressed cytokine levels, with the highest dose (60 μg) showing the most pronounced reduction. Specifically, IL-1β levels were reduced by 21.0% (low-dose), 36.0% (medium-dose), and 43.3% (high-dose), IL-6 levels decreased by 17.9%, 41.3%, and 60.3%, and

TNF-α levels were lowered by 21.6%, 38.1%, and 51.9%, respectively. These results indicate that ESK administration was associated with reduced inflammatory cytokine levels in a dose-dependent fashion.

The findings of WB analysis further confirmed these results (**Figure 4D to G**) by revealing significantly overexpressed cytokine levels in the BCP + Vehicle group compared to the Sham group. The ESK treatment resulted in a significant, dose-dependent reduction in these inflammatory markers, with the high-dose group showing the greatest reduction. Densitometric analysis results elucidated that IL-1β expression in the BCP group was 4.18-fold higher than in the Sham group, while IL-6 and TNF-α levels were 3.48-fold and 3.65-fold higher, respectively. Following ESK administration, IL-1β expression decreased by 22.4% (low-dose), 37.1% (medium-dose), and 65.2% (high-dose), IL-6 expression was reduced by 14.4%, 44.2%, and 58.2%, and TNF-α expression decreased by 23.1%, 54.4%, and 61.5%. IF (**Figure 4H-J**) showed strong fluorescence signals for IL-1β, IL-6 and TNF-α in the SDH of BCP + Vehicle rats. In ESK-treated groups, fluorescence intensity was reduced in a dose-dependent manner. Quantitative analysis (**Figure 4K)** supported significantly lower cytokine signals compared with the BCP + Vehicle group.

3.5. ESK inhibits MAPK pathway activation in the SDH of BCP

rats

The WB outcomes revealed significantly increased JNK (p-JNK), p38 (p-p38), and ERK (p-ERK) phosphorylation levels in the spinal cord of the BCP + Vehicle group compared to the Sham group, indicating MAPK pathway activation in response to BCP (**Figure 5A**). The ESK treatment effectively and dose-dependently reduced the phosphorylation levels of these markers, with the highest dose (60 µg) exerting the most pronounced inhibitory effect (**Figure 5B to D**). Densitometric analysis revealed that p-JNK expression in the BCP group was 2.10-fold higher than in the Sham group, while p-p38 and p-ERK levels were 2.23-fold and 1.99-fold higher, respectively. Following ESK administration, p-JNK expression decreased by 30.8% (low-dose), 40.2% (medium-dose), and 52.9% (high-dose), p-p38 expression was reduced by 26.7%, 34.9%, and 46.3%, and p-ERK expression decreased by 23.4%, 38.1%, and 43.5%, respectively.

Given that ESK inhibited MAPK pathway activation, subsequent analyses specifically focused on the p38 and JNK branches due to their critical roles in glial activation and neuroinflammatory signaling. This approach aimed to elucidate whether ESK's analgesic effects are mediated through modulation of glia-related MAPK activity. To further assess the functional relevance of MAPK signaling in BCP,

pharmacological inhibition of p38 and JNK was conducted using SB203580 and SP600125, respectively. These inhibitors were intrathecally administered alone or in combination with ESK from POD13 to 16 (**Figure 5E**). Behavioral testing showed that both inhibitors partially alleviated mechanical allodynia, as evidenced by increased PWT (**Figure 5F**). Notably, co-administration of MAPK inhibitors did not significantly enhance ESK's analgesic effect. Western blotting of spinal cord tissue revealed that SB203580 and SP600125 treatments decreased the expression of IL-1β, IL-6, and TNF-α (**Figure 5G to J**), mirroring the cytokine-suppressing effect observed with ESK treatment. These results suggest that MAPK p38/JNK activation is associated with cytokine upregulation in BCP, and that ESK may exert part of its effect through inhibition of this pathway.

Discussion

The present study showed that ESK alleviates BCP in a dose-dependent manner, with improvements in pain hypersensitivity, gait performance, and anxiety-like behaviors. Mechanistically, we suggest that ESK exerts its analgesic impacts by inhibiting microglial and astrocytic activation, suppressing pro-inflammatory cytokine release, and downregulating the MAPK signaling pathway in the SDH.

Moreover, while our findings primarily highlight the role of MAPK signaling inhibition, it is important to consider that ESK's analgesic effects may also involve additional mechanisms. As a potent NMDA receptor antagonist[8], ESK is capable of reducing neuronal excitability and attenuating central sensitization, both of which are critical contributors to the pathogenesis and persistence of chronic pain. This complementary mechanism suggests that ESK may simultaneously modulate neuronal and glial activities, providing a broader basis for its analgesic efficacy in BCP.

The successful BCP model establishment was validated by 3D-CT imaging, H&E staining, and pain behavioral tests, which demonstrated osteolytic bone destruction and significant pain hypersensitivity. As expected, BCP rats displayed lowered PWT and PWL, altered gait parameters, and anxiety-like behaviors, all of which are consistent with previous reports on the pathophysiology of BCP[33, 34]. The ESK administration dose-dependently reversed these behavioral deficits, with the highest dose (60 µg) showing the most pronounced analgesic effects. These findings suggest that ESK not only attenuates pain perception but also improves locomotor function and emotional state, which are critical factors impacting the quality of life in cancer patients.

Glial activation in the spinal cord is indispensable in BCP development and maintenance[35]. Once activated, microglia and astrocytes release pro-inflammatory cytokines, contributing to central sensitization and persistent pain states[36]. Consistent with previous studies, our results showed significantly overexpressed Iba-1 and GFAP in the BCP group, indicating robust microglial and astrocytic activation[37]. The administration of ESK dose-dependently and significantly suppressed Iba-1 and GFAP expression, indicating that its analgesic effects may partially result from the inhibition of glial activation. Notably, microglial inhibition has been identified as a key target for chronic pain therapies, and our study provides further evidence supporting the role of ESK in modulating neuroinflammatory pathways beyond its classical NMDA receptor blockade. To further validate the causal role of glial cells in mediating inflammatory responses, we performed additional experiments using selective glial inhibitors. Continuous intrathecal injection of fluorocitrate (astrocyte inhibitor) and minocycline (microglial inhibitor) significantly attenuated mechanical allodynia and reduced the expression of IL-1β, IL-6, and TNF-α in the SDH. These results provide direct evidence that glial activation contributes to spinal cytokine production during BCP, and that modulation of glial reactivity may represent a key mechanism

underlying the analgesic effects of ESK.

Neuroinflammation is a major driver of BCP, with IL-1β, IL-6 and TNF-α playing pivotal roles in amplifying nociceptive transmission[38]. Our results showed that BCP rats exhibited significantly elevated levels of these cytokines, consistent with previous findings that inflammation-induced hyperalgesia is a hallmark of cancer pain. The ESK administration led to a dose-dependent reduction in IL-1β, IL-6 and TNF-α expression, highlighting its anti-inflammatory potential. This aligns with reports that ESK can modulate immune responses by impeding pro-inflammatory cytokine production. Importantly, chronic pain is often associated with a systemic inflammatory state, and ESK's ability to suppress neuroinflammation suggests that it may have broader implications in managing other inflammatory pain conditions.

The MAPK signaling pathway, including JNK, p38, and ERK, is crucial in regulating glial activation and inflammatory responses in the spinal cord[39]. Our study demonstrated that BCP induced significant p-JNK, p-p38, and p-ERK upregulation, indicating hyperactivation of the MAPK pathway. Previous studies have shown that p-p38 was predominantly expressed in microglia[40], whereas p-JNK was highly localized in astrocytes[39], suggesting distinct roles for different MAPK subtypes in pain pathogenesis. The ESK

administration significantly reduced JNK, p38, and ERK phosphorylation levels, with the most pronounced inhibition observed in the high-dose group. To further confirm the involvement of MAPK signaling in mediating nociceptive and inflammatory responses, we employed selective MAPK inhibitors (SB203580 for p38 and SP600125 for JNK) administered intrathecally, either alone or in combination with ESK. Inhibitor treatment alleviated mechanical allodynia and reduced spinal cytokine expression.—Notably, co-administration of MAPK inhibitors did not significantly enhance the analgesic effect of ESK, indicating that ESK's antinociceptive action is largely, though not exclusively, mediated through inhibition of the MAPK pathway.

Although ESK's effects on pain relief have been extensively studied, its precise mechanisms in modulating glial function remain incompletely understood[41]. Beyond NMDA receptor antagonism, ESK has been shown to influence a range of molecular targets, including opioid receptors, monoamine pathways, and voltage-gated ion channels, all of which may contribute to its analgesic profile[42-44]. Moreover, accumulating evidence suggests that ESK can modulate PI3K/AKT signaling, which is crucial in governing neuroprotection[8].

Given these promising preclinical findings, the clinical translation of ESK for cancer pain management warrants careful consideration. Its

rapid onset of analgesia and dual actions on neuronal excitability and neuroinflammation suggest that ESK may offer advantages over traditional analgesics. However, potential risks, including dissociative symptoms, cognitive impairment, and cardiovascular side effects associated with NMDA receptor antagonists, must be critically evaluated[45-48]. In addition, a more critical discussion of clinical implications is warranted. The potential adverse effects and neurotoxicity of intrathecal ESK, along with the risks of infection, meningitis, and catheter-related complications, should be carefully evaluated to ensure the safety and practicality of this administration route in cancer patients. Future studies should explore alternative delivery methods. Approaches such as nanoparticle-based formulations or sustained-release hydrogels could enhance ESK's therapeutic window while minimizing systemic side effects[49, 50]. Future rigorous clinical trials are essential to validate the therapeutic potential of ESK and to establish evidence-based guidelines for its use in managing cancer-related pain.

Compared to traditional analgesics such as opioids, ESK exhibits a favorable safety profile by reducing the risk of respiratory depression, tolerance development, and opioid-induced hyperalgesia[51]. Furthermore, unlike opioids, ESK has demonstrated rapid-acting

antidepressant effects, which could be particularly beneficial for cancer patients who often suffer from comorbid depression[52]. Additionally, compared to ketamine, another NMDA receptor antagonist widely used for pain management, ESK offers advantages including a lower incidence of psychotomimetic side effects and more predictable pharmacokinetics[53]. While both ESK and ketamine exert analgesic effects through NMDA receptor blockade, ESK's modulation of glial activation and inflammatory pathways, as demonstrated in this study, suggests a broader mechanism of action that may confer additional benefits in managing chronic and cancer-related pain. This multifaceted action positions ESK as a promising candidate in contemporary pain management, particularly for patients who are intolerant or refractory to conventional treatments.

Despite these encouraprior literature, future research should aim to clarify the potential interaction between MAPK and other signaling pathways, such as PI3K/AKT/mTOR, NF-κB, or TLR4, which are also implicated in neuroinflammation and central sensitization in bone cancer pain models[54]. Previous studies have shging findings, several key issues remain unresolved. Based on the current study and own that these pathways may converge on common downstream targets influencing cytokine expression and synaptic plasticity, suggesting

that ESK's analgesic effects may involve broader molecular networks. Furthermore, whether repeated intrathecal administration of ESK may induce pharmacodynamic tolerance or desensitization-similar to opioid-induced tolerance-remains unknown. Long-term animal studies using chronic dosing regimens will be essential to determine the sustainability of analgesic efficacy and to monitor potential neurotoxicity or compensatory glial responses. Lastly, incorporating multi-omics approaches such as transcriptomic or proteomic profiling could help uncover novel molecular targets influenced by ESK, and guide the development of combination strategies that enhance and prolong its therapeutic benefit. Several limitations of this study should be acknowledged. First, all experiments were performed in a rat model of bone cancer pain, and animal models cannot fully capture the complexity of human cancer pain syndromes. Second, only female rats were used, and potential sex-related differences were not addressed. Third, the study focused on a short observation period (up to POD 18), and the long-term efficacy, tolerance, and potential neurotoxicity of repeated intrathecal ESK administration remain to be clarified. Fourth, while MAPK signaling and glial activation were identified as key mechanisms, other relevant pathways such as NF-κB, PI3K/AKT, or TLR4 were not systematically investigated.

In summary, our study provides evidence that ESK effectively alleviates BCP by inhibiting glial activation, reducing neuroinflammatory cytokine production, and suppressing MAPK signaling (**Figure 6**). Supplementary pharmacological experiments further confirm the causal role of glia and MAPK pathways in mediating nociceptive sensitization and inflammatory signaling. Our findings offer innovative perspectives into ESK mechanisms beyond NMDA receptor antagonism, highlighting its potential as a multimodal analgesic in cancer pain treatment. Future research focusing on long-term efficacy, optimal dosing strategies, and alternative molecular pathways will be crucial in further developing ESK as a therapeutic option for chronic pain conditions.

Conclusion

This study demonstrates that ESK alleviates bone cancer pain in a dose-dependent manner by inhibiting glial activation, reducing pro-inflammatory cytokines, and suppressing MAPK signaling in the SDH. Pharmacological validation confirms the involvement of glia and MAPK pathways in ESK's effects. These findings support ESK as a promising multimodal analgesic for cancer pain. Further studies are needed to optimize dosing and evaluate long-term safety for clinical

use.

Data Statement

Acknowledgments

Funding

Author contributions

LC and CX designed the study. DW, ZZ, YZ, YT, KB, BG, KZ, YC, and HR performed the experiments. CX and HN analyzed the data. LC and DW drafted and revised the manuscript. All authors reviewed and approved the final manuscript.

Competing interests

All authors declare no competing interests.

References

1. Hua B, Gao Y, Kong X, et al. New insights of nociceptor sensitization in bone cancer pain. *Expert Opin Ther Targets.* 19:227-243, 2015 doi: 10.1517/14728222.2014.980815

2. Ruivo J, Tavares I, Pozza DH. Molecular targets in bone cancer pain: a systematic review of inflammatory cytokines. *Journal of molecular medicine (Berlin, Germany).* 102:1063-1088, 2024 doi: 10.1007/s00109-024-02464-2

3. Mantyh P. Bone cancer pain: causes, consequences, and therapeutic opportunities. *Pain.* 154 Suppl 1:S54-s62, 2013 doi: 10.1016/j.pain.2013.07.044

4. Wang X, Li L, Wang Y. Mechanisms of Cancer-Induced Bone Pain. *J Pain Res.* 18:315-326, 2025 doi: 10.2147/jpr.S498466

5. Chwistek M. Mitigating the Risk of Aberrant Use of Opioids in Patients With Cancer Pain. *Journal of the National Comprehensive*

Cancer Network : JNCCN. 21:1212-1213, 2023 doi: 10.6004/jnccn.2023.7095

6. Page AJ, Spencer K, Mulvey MR, et al. Non-steroidal anti-inflammatory drugs (NSAIDs) in cancer pain: A database analysis to determine recruitment feasibility for a clinical trial. *Palliative medicine.* 36:1440-1445, 2022 doi: 10.1177/02692163221122263

7. Zhang Q-w, Wang X, Wang Z-y, et al. Low-dose esketamine improves acute postoperative pain in patients undergoing thoracoscopic surgery. *Anesthesiology and Perioperative Science.* 2:5, 2024 doi: 10.1007/s44254-023-00039-x

8. Niu X, Zheng Y, Wang W, et al. Esketamine Provides Neuroprotection After Intracerebral Hemorrhage in Mice via the NTF3/PI3K/AKT Pathway. *CNS Neurosci Ther.* 30:e70145, 2024 doi: 10.1111/cns.70145

9. Wang T, Weng H, Zhou H, et al. Esketamine alleviates postoperative depression-like behavior through anti-inflammatory actions in mouse prefrontal cortex. *Journal of affective disorders.* 307:97-107, 2022 doi: 10.1016/j.jad.2022.03.072

10. Duan C, Zhu Y, Zhang Z, et al. Esketamine inhibits the c-Jun N-terminal kinase pathway in the spinal dorsal horn to relieve bone cancer pain in rats. *Mol Pain.* 20:17448069241239231, 2024 doi: 10.1177/17448069241239231

11. Hu N, Zheng Y, Liu X, et al. CircKat6b Mediates the Antidepressant Effect of Esketamine by Regulating Astrocyte Function. *Mol Neurobiol.* 62:2587-2600, 2025 doi: 10.1007/s12035-024-04420-0

12. Wen Y, Xu J, Shen J, et al. Esketamine Prevents Postoperative Emotional and Cognitive Dysfunction by Suppressing Microglial M1 Polarization and Regulating the BDNF-TrkB Pathway in Ageing

Rats with Preoperative Sleep Disturbance. *Mol Neurobiol.* 61:5680-5698, 2024 doi: 10.1007/s12035-023-03860-4

13. Gao Y, Li L, Zhao F, et al. Esketamine at a Clinical Dose Attenuates Cerebral Ischemia/Reperfusion Injury by Inhibiting AKT Signaling Pathway to Facilitate Microglia M2 Polarization and Autophagy. *Drug design, development and therapy.* 19:369-387, 2025 doi: 10.2147/dddt.S504179

14. Apryani E, Ali U, Wang ZY, et al. The spinal microglial IL-10/β-endorphin pathway accounts for cinobufagin-induced mechanical antiallodynia in bone cancer pain following activation of α7-nicotinic acetylcholine receptors. *J Neuroinflammation.* 17:75, 2020 doi: 10.1186/s12974-019-1616-z

15. Peng Y, Zhang Y, Wang W, et al. Potential role of remimazolam in alleviating bone cancer pain in mice via modulation of translocator protein in spinal astrocytes. *Eur J Pharmacol.* 979:176861, 2024 doi: 10.1016/j.ejphar.2024.176861

16. Zhou YQ, Liu Z, Liu HQ, et al. Targeting glia for bone cancer pain. *Expert Opin Ther Targets.* 20:1365-1374, 2016 doi: 10.1080/14728222.2016.1214716

17. Hennes M, Richter ML, Fischer-Sternjak J, et al. Astrocyte diversity and subtypes: aligning transcriptomics with multimodal perspectives. *EMBO Rep.* 26:4203-4218, 2025 doi: 10.1038/s44319-025-00529-y

18. Yang YJ, Hu L, Xia YP, et al. Resveratrol suppresses glial activation and alleviates trigeminal neuralgia via activation of AMPK. *J Neuroinflammation.* 13:84, 2016 doi: 10.1186/s12974-016-0550-6

19. Uemura Y, Hiroshima Y, Tada A, et al. Porphyromonas gingivalis Outer Membrane Vesicles Stimulate Gingival Epithelial Cells to

Induce Pro-Inflammatory Cytokines via the MAPK and STING Pathways. *Biomedicines.* 10, 2022 doi: 10.3390/biomedicines10102643

20. Shi T, Liu Y, Ji B, et al. Acupuncture Relieves Cervical Spondylosis Radiculopathy by Regulating Spinal Microglia Activation Through MAPK Signaling Pathway in Rats. *J Pain Res.* 16:3945-3960, 2023 doi: 10.2147/jpr.S419927

21. Xu M, Ni H, Xu L, et al. B14 ameliorates bone cancer pain through downregulating spinal interleukin-1β via suppressing neuron JAK2/STAT3 pathway. *Mol Pain.* 15:1744806919886498, 2019 doi: 10.1177/1744806919886498

22. He Q, Liu L, Wang Y, et al. miR-155-5p in the spinal cord regulates hypersensitivity in a rat model of bone cancer pain. *Mol Pain.* 18:17448069221127811, 2022 doi: 10.1177/17448069221127811

23. Xu C, Wang Y, Ni C, et al. Histone modifications and Sp1 promote GPR160 expression in bone cancer pain within rodent models. *EMBO Rep.* 25:5429-5455, 2024 doi: 10.1038/s44319-024-00292-6

24. Lobos N, Lux S, Zepeda RJ, et al. Rosuvastatin Synergistically Enhances the Antinociceptive Efficacy of Duloxetine in Paclitaxel-Induced Neuropathic Pain in Mice. *Int J Mol Sci.* 24, 2023 doi: 10.3390/ijms24098359

25. Hu XM, Yang W, Du LX, et al. Vascular Endothelial Growth Factor A Signaling Promotes Spinal Central Sensitization and Pain-related Behaviors in Female Rats with Bone Cancer. *Anesthesiology.* 131:1125-1147, 2019 doi: 10.1097/aln.0000000000002916

26. Sun L, Ma S, Yu Y, et al. Transcutaneous auricular vagus nerve

stimulation ameliorates adolescent depressive- and anxiety-like behaviors via hippocampus glycolysis and inflammation response. *CNS Neurosci Ther.* 30:e14614, 2024 doi: 10.1111/cns.14614

27. Xu M, Fei Y, He Q, et al. Electroacupuncture Attenuates Cancer-Induced Bone Pain via NF-κB/CXCL12 Signaling in Midbrain Periaqueductal Gray. *ACS Chem Neurosci.* 12:3323-3334, 2021 doi: 10.1021/acschemneuro.1c00224

28. Ni HD, Yao M, Huang B, et al. Glial activation in the periaqueductal gray promotes descending facilitation of neuropathic pain through the p38 MAPK signaling pathway. *Journal of neuroscience research.* 94:50-61, 2016 doi: 10.1002/jnr.23672

29. Ni H, Wang Y, An K, et al. Crosstalk between NFκB-dependent astrocytic CXCL1 and neuron CXCR2 plays a role in descending pain facilitation. *J Neuroinflammation.* 16:1, 2019 doi: 10.1186/s12974-018-1391-2

30. Ni H, Xu M, Kuang J, et al. Upregulation of LncRNA71132 in the spinal cord regulates hypersensitivity in a rat model of bone cancer pain. *Pain.* 164:180-196, 2023 doi: 10.1097/j.pain.0000000000002678

31. Wang C, Xu K, Wang Y, et al. Spinal cannabinoid receptor 2 activation reduces hypersensitivity associated with bone cancer pain and improves the integrity of the blood-spinal cord barrier. *Regional anesthesia and pain medicine.* 45:783-791, 2020 doi: 10.1136/rapm-2019-101262

32. Fuseya S, Yamamoto K, Minemura H, et al. Systemic QX-314 Reduces Bone Cancer Pain through Selective Inhibition of Transient Receptor Potential Vanilloid Subfamily 1-expressing Primary Afferents in Mice. *Anesthesiology.* 125:204-218, 2016 doi:

10.1097/aln.0000000000001152

33. Chen L, Hua B, He Q, et al. Curcumin analogue NL04 inhibits spinal cord central sensitization in rats with bone cancer pain by inhibiting NLRP3 inflammasome activation and reducing IL-1β production. *Eur J Pharmacol.* 970:176480, 2024 doi: 10.1016/j.ejphar.2024.176480

34. Li Y, Zheng G, Tang Y, et al. Naringenin alleviates bone cancer pain via NF-κB/uPA/PAR2 pathway in mice. *Journal of orthopaedic surgery (Hong Kong).* 32:10225536241266671, 2024 doi: 10.1177/10225536241266671

35. Zhou YS, Cui Y, Zheng JX, et al. Luteolin relieves lung cancer-induced bone pain by inhibiting NLRP3 inflammasomes and glial activation in the spinal dorsal horn in mice. *Phytomedicine.* 96:153910, 2022 doi: 10.1016/j.phymed.2021.153910

36. Ji RR, Nackley A, Huh Y, et al. Neuroinflammation and Central Sensitization in Chronic and Widespread Pain. *Anesthesiology.* 129:343-366, 2018 doi: 10.1097/aln.0000000000002130

37. Ni H, Xu M, Xie K, et al. Liquiritin Alleviates Pain Through Inhibiting CXCL1/CXCR2 Signaling Pathway in Bone Cancer Pain Rat. *Front Pharmacol.* 11:436, 2020 doi: 10.3389/fphar.2020.00436

38. Saadh MJ, Rashed AB, Jamal A, et al. miR-199a-3p suppresses neuroinflammation by directly targeting MyD88 in a mouse model of bone cancer pain. *Life Sci.* 333:122139, 2023 doi: 10.1016/j.lfs.2023.122139

39. Ni HD, Xu LS, Wang Y, et al. Astrocyte activation in the periaqueductal gray promotes descending facilitation to cancer-induced bone pain through the JNK MAPK signaling pathway. *Mol

Pain. 15:1744806919831909, 2019 doi: 10.1177/1744806919831909

40. Kiyomoto M, Shinoda M, Honda K, et al. p38 phosphorylation in medullary microglia mediates ectopic orofacial inflammatory pain in rats. *Mol Pain.* 11:48, 2015 doi: 10.1186/s12990-015-0053-y

41. Zhao H, Li Z. Analgesic Mechanism of Dexmedetomidine and Esketamine in Rats with Spinal Cord Injury. *Discovery medicine.* 36:714-720, 2024 doi: 10.24976/Discov.Med.202436183.67

42. Xu J, Li M, Hu Y, et al. Esketamine reduces postoperative depression in breast cancer through TREK-1 channel inhibition and neurotransmitter modulation. *Cancer cell international.* 25:51, 2025 doi: 10.1186/s12935-025-03664-7

43. Witkin JM, Cerne R, Newman AH, et al. N-Substituted-3-alkoxy-derivatives of dextromethorphan are functional NMDA receptor antagonists in vivo: Evidence from an NMDA-induced seizure model in rats. *Pharmacology, biochemistry, and behavior.* 203:173154, 2021 doi: 10.1016/j.pbb.2021.173154

44. Levinstein MR, Budinich RC, Bonaventura J, et al. Redefining Ketamine Pharmacology for Antidepressant Action: Synergistic NMDA and Opioid Receptor Interactions? *The American journal of psychiatry.*appiajp20240378, 2025 doi: 10.1176/appi.ajp.20240378

45. Vankawala J, Naples G, Avila-Quintero VJ, et al. Meta-Analysis: Hemodynamic Responses to Sub-anesthetic Doses of Ketamine in Patients With Psychiatric Disorders. *Frontiers in psychiatry.* 12:549080, 2021 doi: 10.3389/fpsyt.2021.549080

46. Stahl SM, De Martin S, Mattarei A, et al. Esmethadone (REL-1017) and Other Uncompetitive NMDAR Channel Blockers May Improve

Mood Disorders via Modulation of Synaptic Kinase-Mediated Signaling. *Int J Mol Sci.* 23, 2022 doi: 10.3390/ijms232012196

47. Miao Y, Zheng M, Li Q, et al. Comparison of propofol-esketamine versus propofol-sufentanil for deep sedation and analgesia in children with autism: A randomized double-blind clinical trial. *Autism research : official journal of the International Society for Autism Research.* 17:1356-1364, 2024 doi: 10.1002/aur.3172

48. Duan JJ, Jiang B, Yin W, et al. Cell-autonomous GABAARs are essential for NMDAR-mediated synaptic transmission, LTP, and spatial memory. *EMBO Rep.* 26:4456-4476, 2025 doi: 10.1038/s44319-025-00538-x

49. Ma K, Pham T, Wang J, et al. Nanoparticle-based inhibition of vascular endothelial growth factor receptors alleviates osteoarthritis pain and cartilage damage. *Science advances.* 10:eadi5501, 2024 doi: 10.1126/sciadv.adi5501

50. Khanal M, Gohil SV, Kuyinu E, et al. Injectable nanocomposite analgesic delivery system for musculoskeletal pain management. *Acta biomaterialia.* 74:280-290, 2018 doi: 10.1016/j.actbio.2018.05.038

51. Yan H, Chen W, Chen Y, et al. Opioid-Free Versus Opioid-Based Anesthesia on Postoperative Pain After Thoracoscopic Surgery: The Use of Intravenous and Epidural Esketamine. *Anesthesia and analgesia.* 137:399-408, 2023 doi: 10.1213/ane.0000000000006547

52. Lewis V, Rurak G, Salmaso N, et al. An integrative view on the cell-type-specific mechanisms of ketamine's antidepressant actions. *Trends Neurosci.* 47:195-208, 2024 doi: 10.1016/j.tins.2023.12.004

53. Hung KC, Kao CL, Ho CN, et al. The impact of perioperative ketamine or esketamine on the subjective quality of recovery after surgery: a meta-analysis of randomised controlled trials. *Br J Anaesth.* 132:1293-1303, 2024 doi: 10.1016/j.bja.2024.03.012

54. Zhang H, Jiang J, Chen X, et al. Liu-Shen-Wan inhibits PI3K/Akt and TRPV1 signaling alleviating bone cancer pain in rats. *Cancer biology & therapy.* 25:2432098, 2024 doi: 10.1080/15384047.2024.2432098

Figure 1. BCP Model Establishment and ESK Dose-dependent Analgesic Effects

(A) Experimental timeline illustrating BCP surgery, followed by behavioral assessments of mechanical allodynia and thermal hyperalgesia. **(B)** 3D-CT images: Tumor-induced osteolysis in the affected tibia. **(C)** H&E staining of the tibia: Bone destruction and tumor infiltration in the BCP model. Scale bar: 50 µm. **(D–E)** Behavioral assessments: Pain hypersensitivity in sham and BCP rats. Significantly decreased PWT (D) and PWL (E) in BCP rats vs. sham-operated controls. Data are mean ± SEM of biological replicates n = 7–8 rats/group. Two-way ANOVA with repeated measures followed by post hoc Tukey test. $**P < 0.01$, $***P < 0.001$ versus Sham group. **(F–H)** Intrathecal administration of ESK (20, 40, and 60 µg) dose-dependently mitigated PWT (F) and PWL (G). Compared to baseline performance, intrathecal administration of ESK over four consecutive days did not alter motor function (H). Data are mean ± SEM of biological replicates n = 7–8 rats/group. Two-way ANOVA with repeated measures followed by post hoc Tukey test. $*P < 0.05$, $**P < 0.01$, $***P < 0.001$ vs. BCP + Vehicle; $^{\#}P < 0.05$ vs. BCP + ES-2 at corresponding time points. **(I–K)** Representative double immunofluorescence images showing Iba-1 (green), GFAP (red), and

DAPI (blue) in the SDH (I). Iba-1 expression increased from POD6 and remained elevated through POD18, while GFAP expression was significantly upregulated at POD12 and POD18. Quantification of fluorescence intensity (J, K) confirms these changes. Scale bars: 50 μm. Data are mean ± SEM of biological replicates n = 3. *P < 0.05, **P < 0.01, ***P < 0.001 vs. Sham, One-way ANOVA with repeated measures followed by post hoc Tukey test.

Figure 2. ESK Improves Gait Performance and Anxiety-like Behavior

(A) CatWalk: Gait patterns, displaying print view, foot pattern, print intensity, and timing view. **(B-E)** Quantification of gait alterations: Maximum contact area (B), mean intensity (C), single stance duration (D), and swing duration (E) of the left hind paw compared to the right hind paw. **(F)** Representative open field test (OFT): Tracks in the three groups, with the central area indicating in red. **(G–H)** Quantification of OFT parameters: Percentage of total distance traveled and (G) total time spent in the central area (H). Data are mean ± SEM of biological replicates n = 8. *P < 0.05, ***P < 0.001, One-way ANOVA with repeated measures followed by post hoc Tukey test.

Figure 3. ESK dose-dependently inhibits microglia and

astrocyte activation

(A-C) Representative immunofluorescence images showing Iba-1 (green), GFAP (red), and DAPI (blue) expression in the SDH across treatment groups (A). Esketamine dose-dependently reduced glial activation. Data are mean ± SEM of biological replicates n = 3. ***P < 0.001 vs. sham plus vehicle group; #P < 0.05, ##P < 0.01, ###P < 0.001 vs. BCP + vehicle group, One-way ANOVA with repeated measures followed by post hoc Tukey test. Scale bars: 50 µm. **(D)** Representative Western blot (WB) images: GFAP and Iba-1 protein levels in different groups. **(E–F)** Quantification of WB: Iba-1 (E) and GFAP (F) normalized to β-actin. Data are mean ± SEM of biological replicates n = 3. ***P < 0.001 vs. sham group; #P < 0.05, ##P < 0.01, ###P < 0.001 vs. BCP + vehicle group, One-way ANOVA with repeated measures followed by post hoc Tukey test. (**G**) Intrathecal injection of fluorocitrate (astrocyte inhibitor) and minocycline (microglial inhibitor) increased PWT on POD 13 to 16. Data are mean ± SEM of biological replicates n = 7–8/group. *P < 0.05 vs. BCP + Saline at corresponding time points, One-way ANOVA with repeated measures followed by post hoc Tukey test. (**H-I**) Immunofluorescence showed reduced GFAP (H) and Iba-1 (I) expression in the SDH following glial inhibition. Scale bar = 50 µm. (**J-K**) Quantification of GFAP and Iba-1

fluorescence intensity. Student's unpaired t test, Data are mean ± SEM of biological replicates n = 3, *$P < 0.05$ versus saline group. (**L**) Western blotting image of IL-1β, IL-6, and TNF-α expression. (**M–O**) Western blotting quantitative analysis showed decreased cytokine levels after glial inhibition. Data are mean ± SEM of biological replicates n = 3. *$P < 0.05$, **$P < 0.01$ vs. BCP + Saline. ns, not significant, One-way ANOVA with repeated measures followed by post hoc Tukey test.

Figure 4 ESK dose-dependently downregulates pro-inflammatory cytokines

(**A-C**) ELISA quantification of IL-1β (A), IL-6 (B), and TNF-α (C) levels in the SDH across different treatment groups. Data are mean ± SEM of biological replicates n = 3 rats/group. ***$P < 0.001$ versus sham plus vehicle group, #$P < 0.05$, ##$P < 0.01$, ###$P < 0.001$ versus BCP plus vehicle group, One-way ANOVA with repeated measures followed by post hoc Tukey test. (**D**) Representative WB images of IL-1β, IL-6, and TNF-α expression in the SDH. (**E-G**) Densitometric analysis of WB results for IL-1β (E), IL-6 (F), and TNF-α (G) normalized to β-actin. Data are mean ± SEM of biological replicates n = 3 rats/group. ***P < 0.001 versus sham plus vehicle group, #$P < 0.05$, ##$P < 0.01$, ###P

< 0.001 versus BCP plus vehicle group, ns, not significant. One-way ANOVA with repeated measures followed by post hoc Tukey test. **(H-J)** Representative IF images showing IL-6 (H), IL-1β (I), and TNF-α (J) expression in the SDH, with DAPI counterstaining for nuclei. Scale bar: 50 μm. **(K)** Quantification of mean IF intensity for IL-6, IL-1β, and TNF-α. Data are mean ± SEM of biological replicates n = 3 rats/group. *P< 0.05, **P< 0.01 versus BCP plus vehicle group, One-way ANOVA with repeated measures followed by post hoc Tukey test.

**Figure 5 ESK inhibits MAPK pathway activation in the SDH of BCP rats**

(**A-D**) Representative WB images and quantification of phosphorylated JNK (B), p38 (C), and ERK (D) levels. Data are mean ± SEM of biological replicates n = 3. ***P < 0.001 versus sham plus vehicle group, #P < 0.05, ##P < 0.01, ###P < 0.001 versus BCP plus vehicle group, ns, not significant. One-way ANOVA with repeated measures followed by post hoc Tukey test. (**E**) Schematic of experimental timeline showing repeated intrathecal administration of ESK, SB203580 (p38 inhibitor), or SP600125 (JNK inhibitor) on POD 13 to 16. (**F**) Co-treatment with ESK enhanced the MAPK inhibitors induced increase in PWT after intrathecal administration. Notably, co-

administration of MAPK inhibitors did not further enhance ESK's analgesic effect, suggesting that its antinociceptive action mainly involves MAPK pathway inhibition. Data are mean ± SEM of biological replicates n = 7–8 rats/group. Two-way ANOVA with repeated measures followed by post hoc Tukey test. *$P < 0.05$, **$P < 0.01$, ***$P < 0.001$ vs. BCP + DMSO; #$P < 0.05$, BCP+ ESK+SB203580 vs. BCP + SB203580, BCP+ ESK+SP600125 vs. BCP + SP600125 at corresponding time points. (**G**) Western blot of IL-1β, IL-6, and TNF-α expression in the SDH. (**H-J**) Quantification of cytokine levels showed further reductions in IL-1β (H), IL-6 (I), and TNF-α (J) with combined ESK and MAPK inhibitor treatment. Data are mean ± SEM of biological replicates n = 3. *$P < 0.05$, **$P < 0.01$, ***$P < 0.001$, ns, not significant. One-way ANOVA with repeated measures followed by post hoc Tukey test.

Figure 6 ESK inhibits the activation of microglia and astrocytes in the SDH of rats
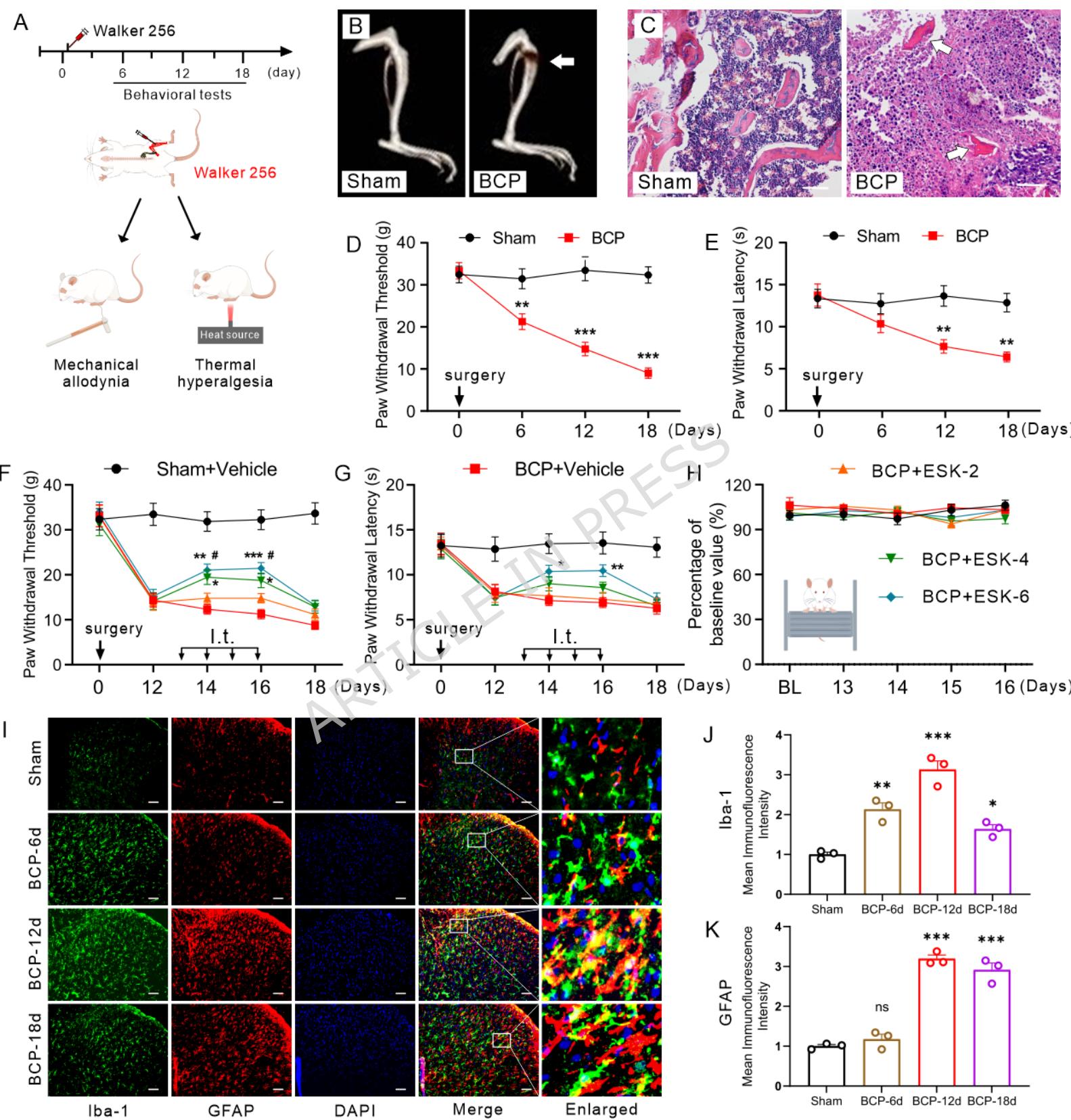
ARTICLE IN PRESS
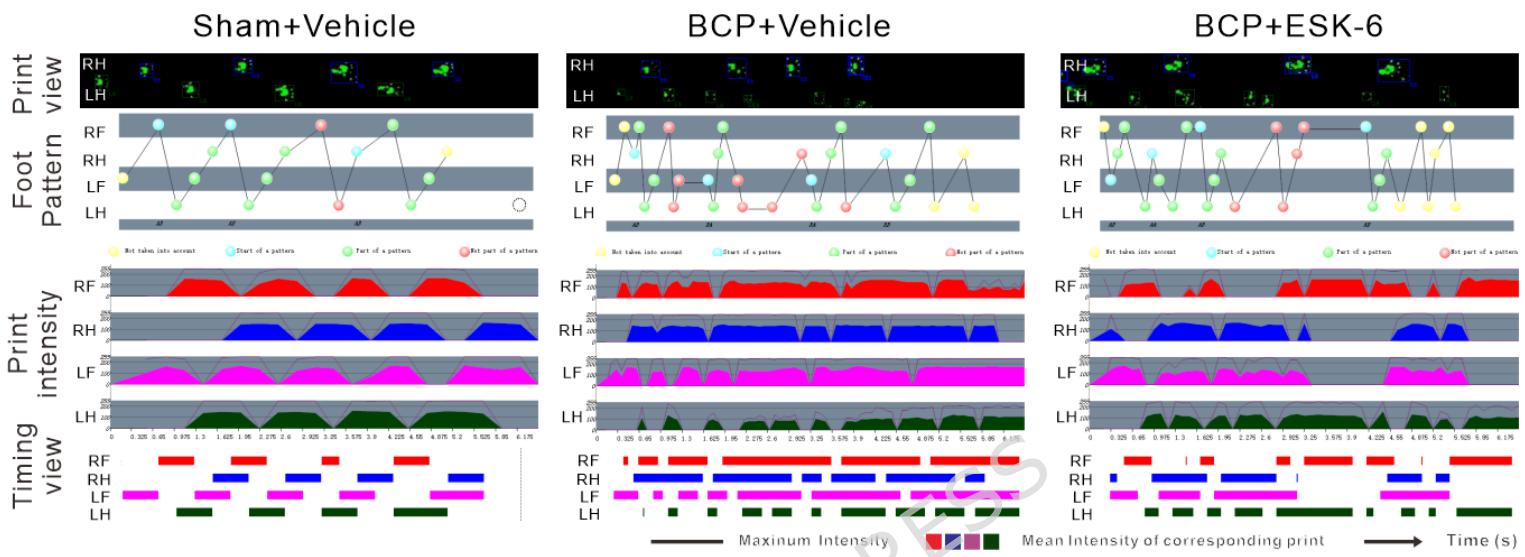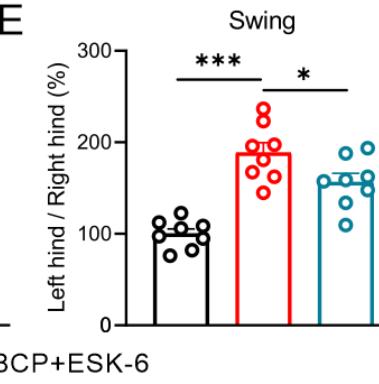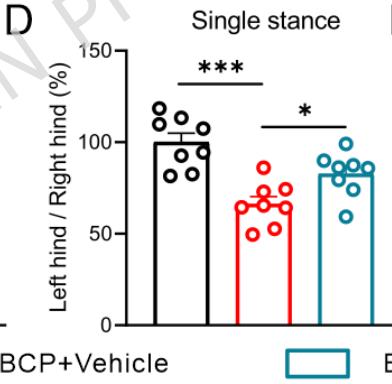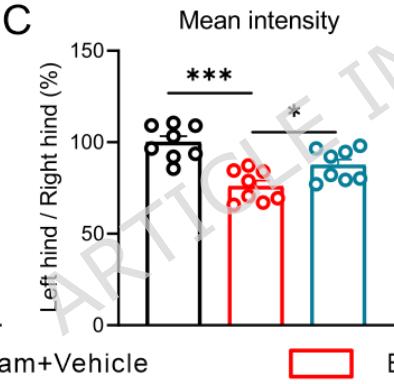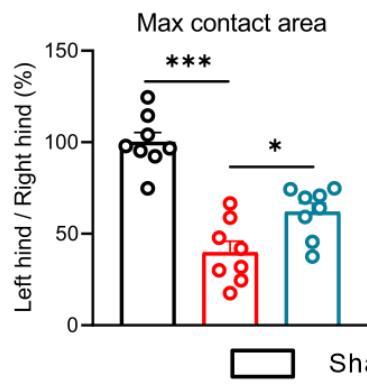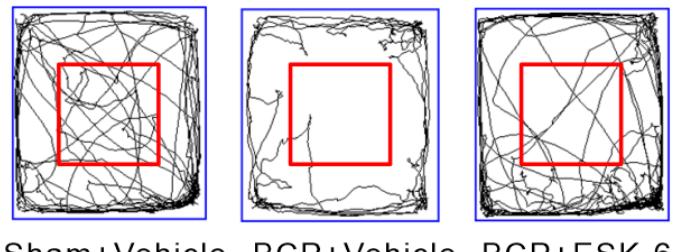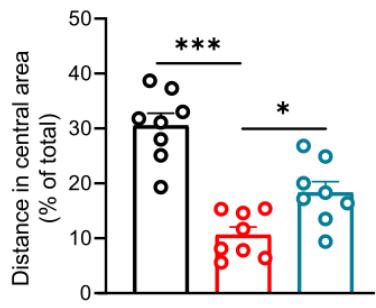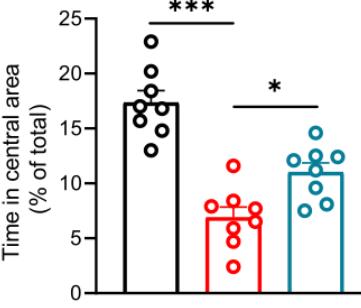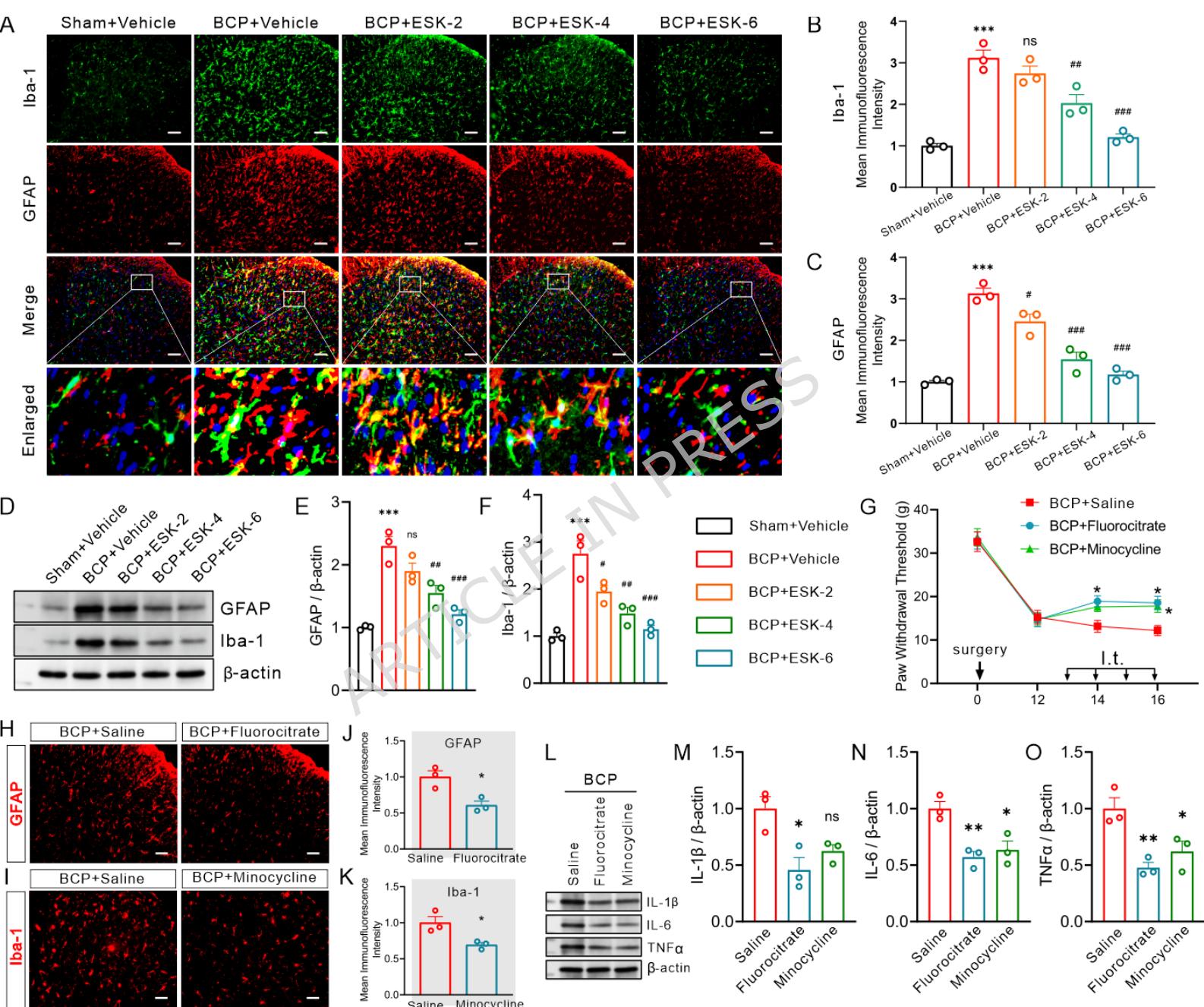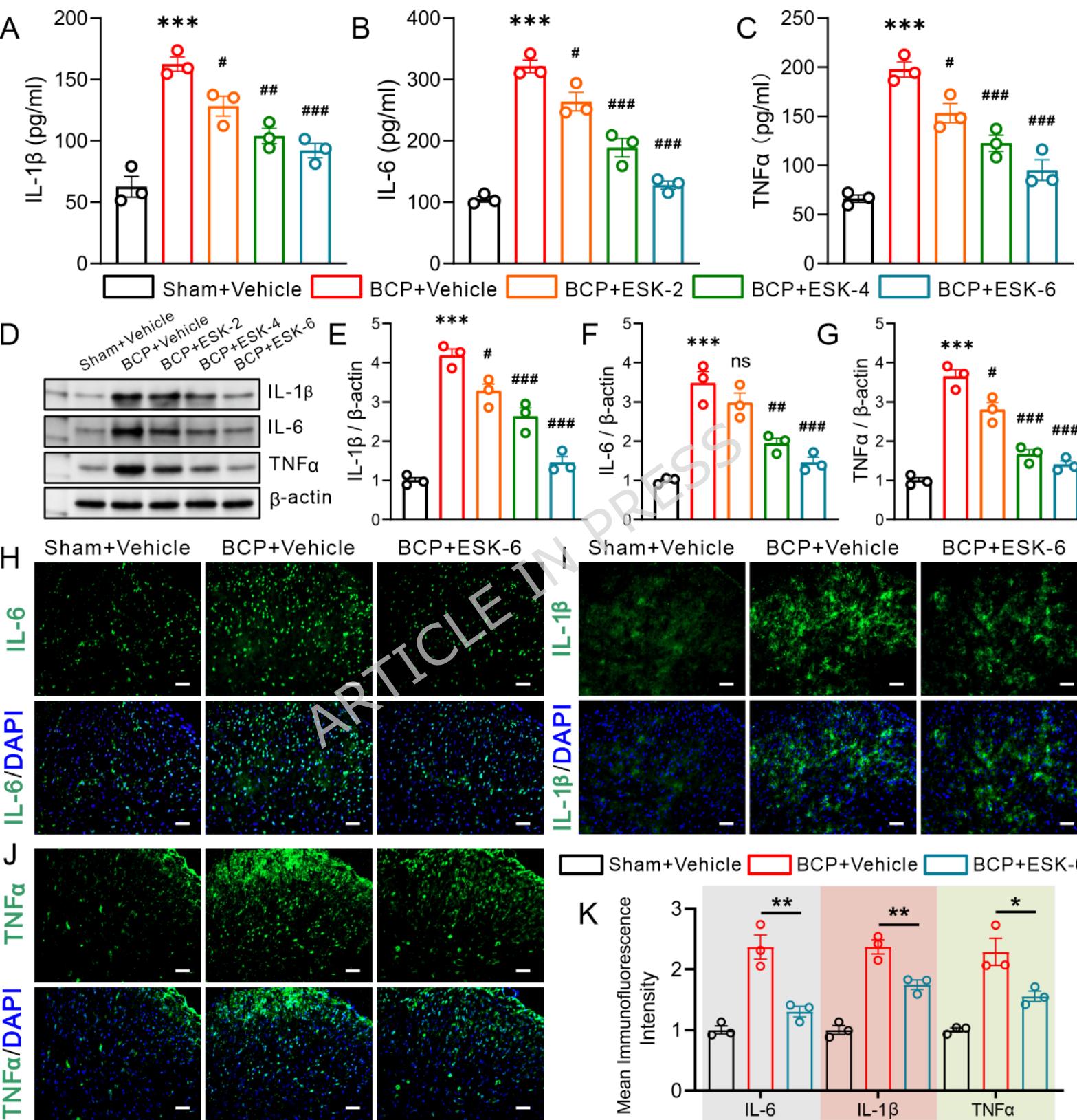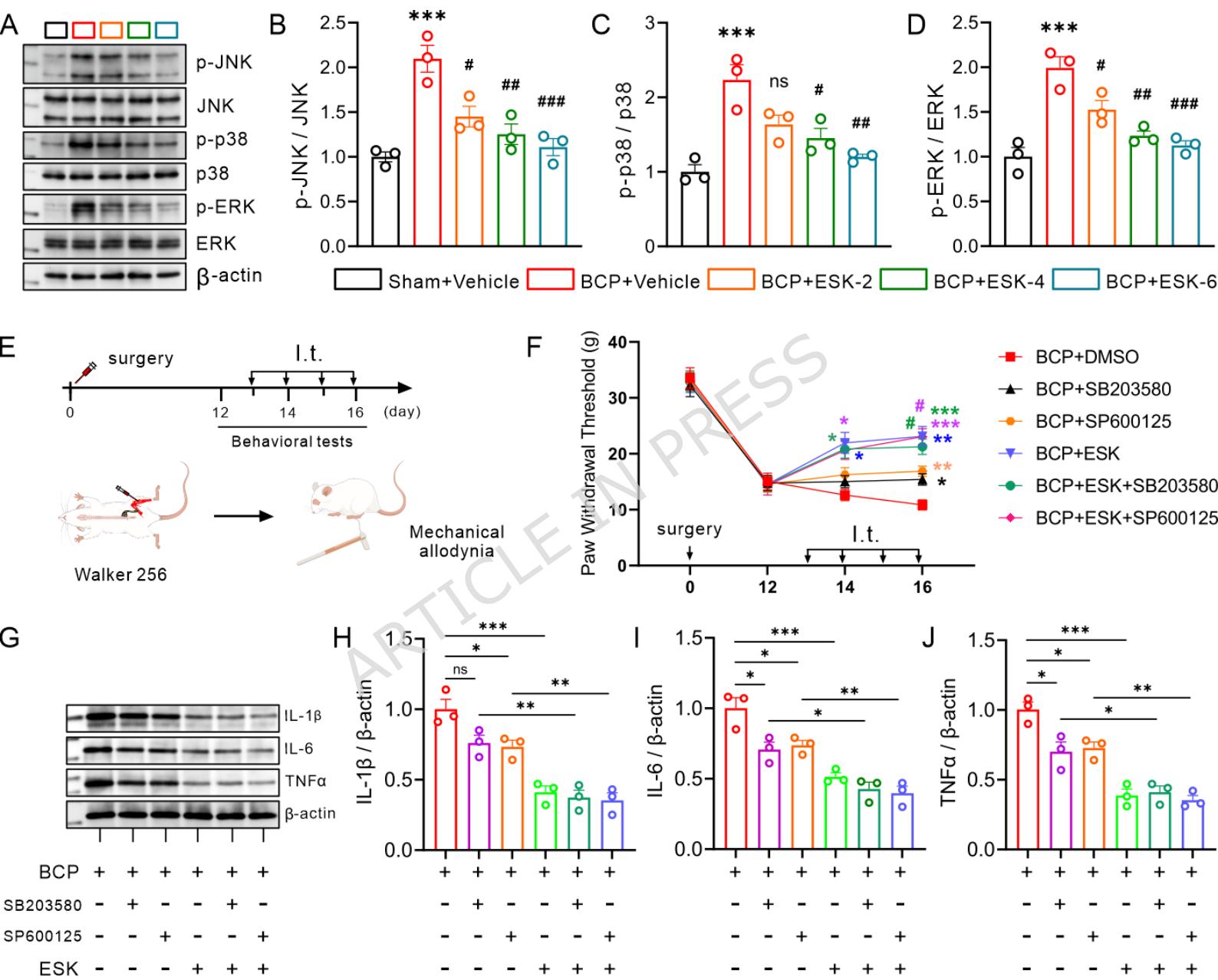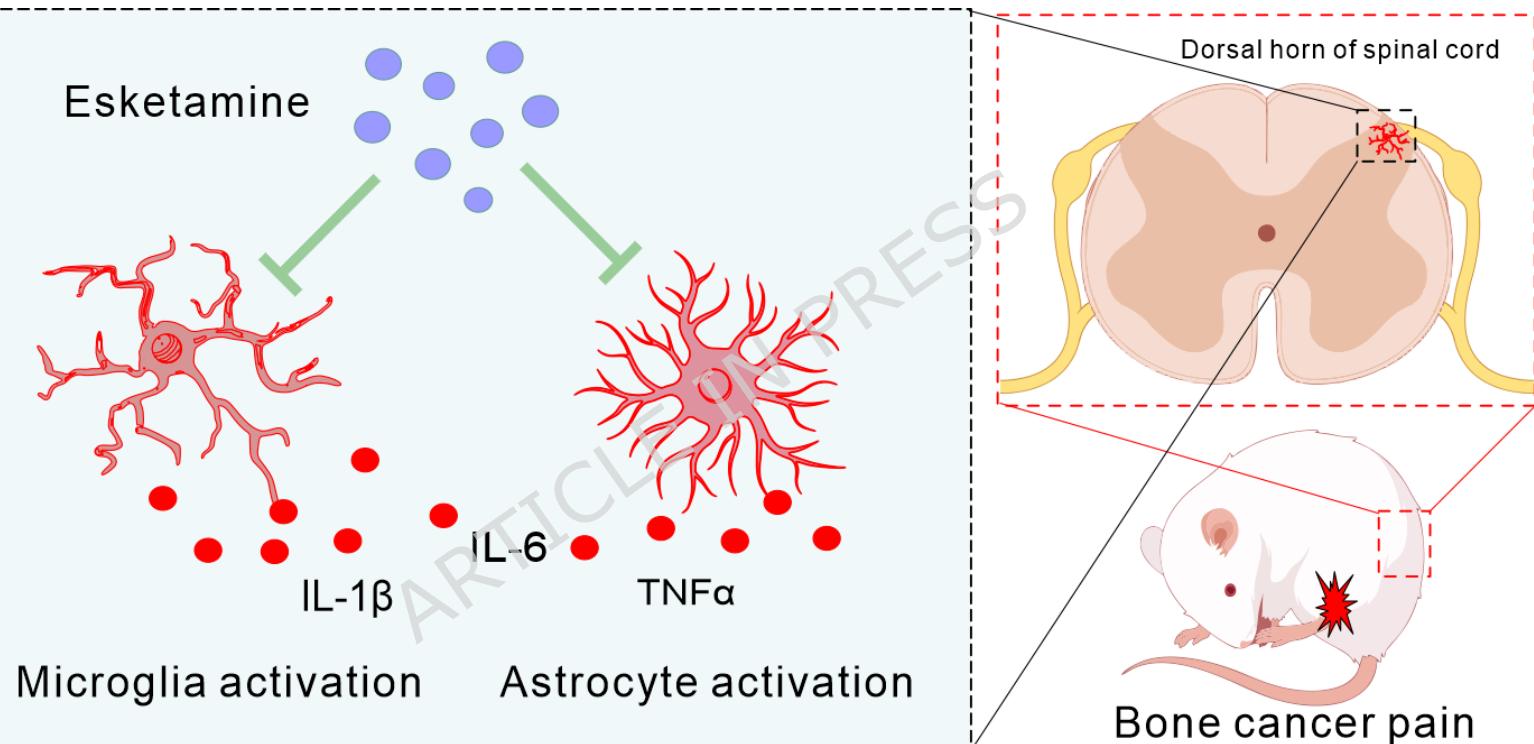
A

Sham+Vehicle

BCP+Vehicle

BCP+ESK-6

Print view: RH, LH

Foot Pattern: RF, RH, LF, LH

Not taken into account | Start of a pattern | Part of a pattern | Not part of a pattern

Print intensity: RF, RH, LF, LH

Timing view: RF, RH, LF, LH

Maximum Intensity | Mean Intensity of corresponding print | Time (s)

B — Max contact area
C — Mean intensity
D — Single stance
E — Swing

Left hind / Right hind (%)

*** *

Sham+Vehicle | BCP+Vehicle | BCP+ESK-6

F

Sham+Vehicle | BCP+Vehicle | BCP+ESK-6

G — Distance in central area (% of total)
H — Time in central area (% of total)

*** *

Esketamine Attenuates Bone Cancer Pain by Suppressing MAPK Signaling and Glial Activation in The Spinal Dorsal Horn of Rats

Table 1 Tumor size and body weight at different time points in the rat BCP model.

	BCP-0d	BCP-6d	BCP-12d	BCP-18d
Tumor measurements (mm)	0*0	5.2*4.1	11.4*9.7	18.1*16.4
Rat weights (g)	186.4±4.6	231.7±4.9	277.3±5.2	301±5.7